Calculations on the Ruthenium-Catalyzed Diene and Dienyne Ring-Closing Metathesis Reactions in the Synthesis of Taxol Derivatives

Samantha Brooks, Georgina Charlton, Aurélien Letort, Joëlle Prunet and Götz Bucher*[a]*

[a]WestCHEM, School of Chemistry, University of Glasgow, Joseph-Black-Building, University Avenue, Glasgow G12 8QQ, United Kingdom. E-mail: joelle.prunet@glasgow.ac.uk; goetz.bucher@glasgow.ac.uk.

Abstract

Density-functional and semiempirical calculations (M06, M06L, and PM6) on intermediates in the ring-closing metathesis reactions in the synthesis of Taxol derivatives give results in excellent agreement with the results of previous experimental work. The results suggest that the degree of steric overloading plays a decisive role in determining the outcome (ene-ene or ene-yne-ene metathesis). Due to the rigidity of the Taxol skeleton being formed in the ene-yne-ene cascade reaction, the transition states in its final ene-ene metathesis reaction stage are particularly sensitive to steric effects. Thus, the reaction is predicted to be preferred for one diastereomer of the precursor in which the diol functionality is protected with a compact cyclic carbonate moiety, whereas the use of a bulkier benzoate protecting group results in activation barriers for Taxol formation that are prohibitive. The reason why one diastereomer of the carbonate-protected precursor undergoes formation of a tricycle via an ene-yne-ene ring closing metathesis cascade, whereas the other diastereomer undergoes cyclooctene formation via an ene-ene RCM likely lies in the orientation of the pseudoaxial methyl group on the cyclohexene ring, which in the latter case would unfavourably point toward the reactive centre of the Ru-complex leading to Taxol formation.

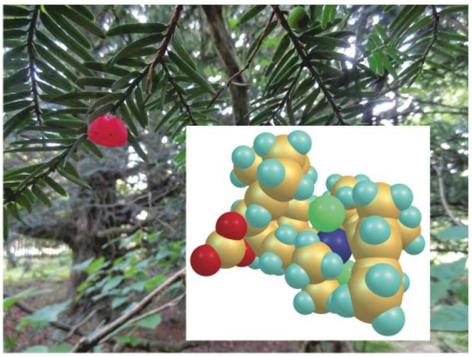

Introduction

Taxol® (paclitaxel) is one of the most affordable and best-selling anticancer drugs; it was approved by the FDA in 1992 and is prescribed nowadays in generic form or as the albumin-bound Abraxane®, which generated more than 1 billion USD in sales in the year 2020 alone. [1] Taxol® (paclitaxel) and its analogues Taxotere® (docetaxel) and Jevtana® (cabazitaxel) are prescribed for the treatment of a broad range of malignancies (Figure 1).[2] Although Taxol is currently manufactured through plant cell fermentation and Taxotere and Jevtana produced by semisynthesis from 10-deacetylbaccatin III, there is

still a need for an efficient synthesis of taxoid derivatives. Seven total syntheses[3] and three formal syntheses[4] of Taxol have been reported, but they all feature at least 37 steps.

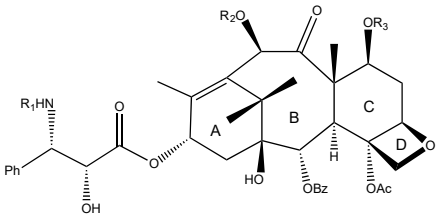

Taxol $R_1 = C_6H_5CO$, R_2 = Ac, R_3 = H
Taxotere R_1 = t-BuOCO, R_2 = H, R_3 = H
Jevtana R_1 = t-BuOCO, R_2 = Me, R_3 = Me

Figure 1: Structure of Taxol and its analogues Taxotere and Jevtana.

During our studies towards the synthesis of the ABC tricycle of Taxol,[5] we developed a cascade dienyne metathesis reaction that forms the A and B rings in one operation. The outcome of this metathesis reaction dramatically depends on the configuration of the C1 and C2 stereocenters and on the diol protecting group at these positions (Scheme 1).[6] Indeed, only substrate **1a'**, which possesses the required configuration for Taxol at C1 and C2 and a carbonate protecting group leads to the desired tricycle **3a'**. The other substrates only undergo simple diene metathesis reactions, giving the undesired bicyclic systems.

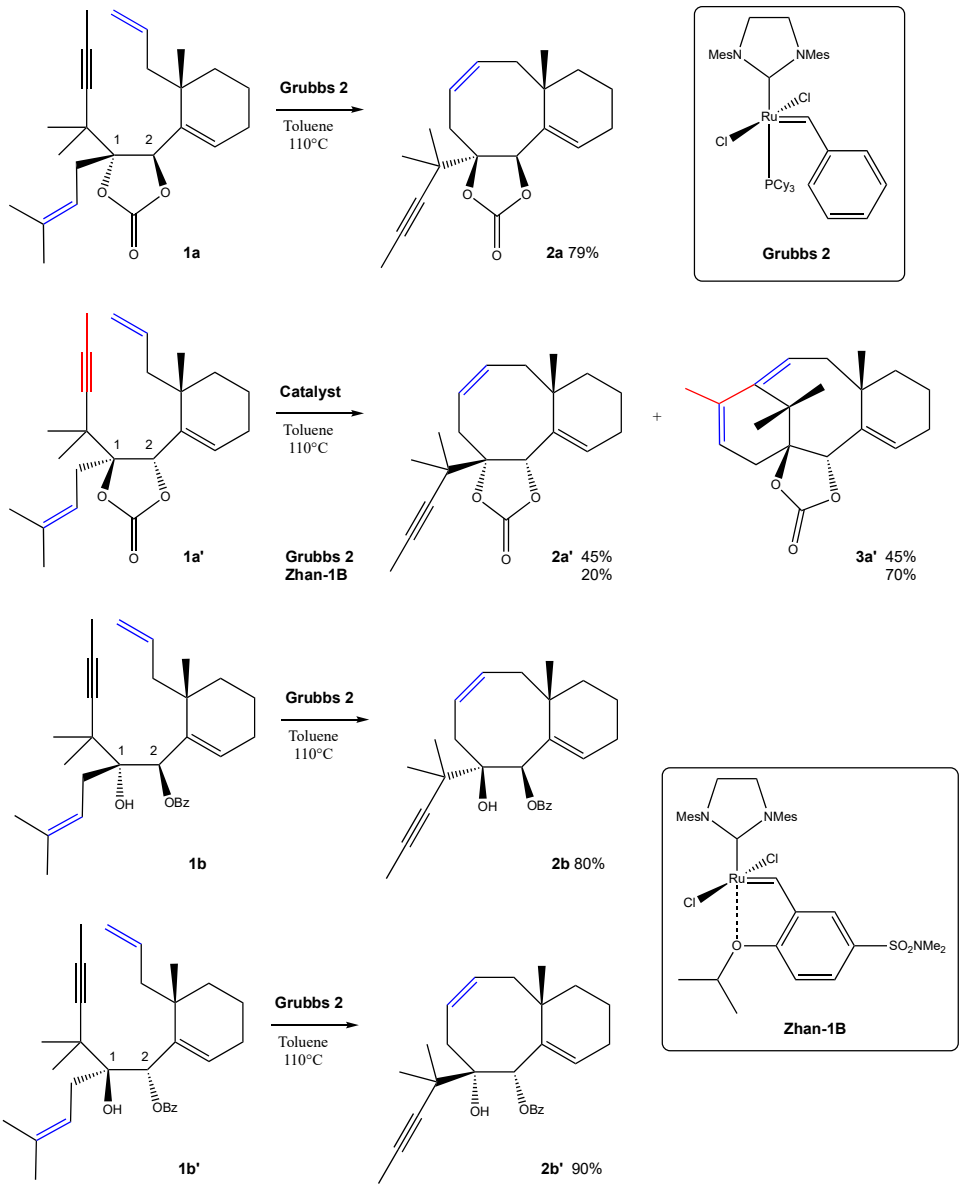

Scheme 1: Diene and dienyne metathesis reactions for the synthesis of an intermediate of Taxol

In order to better understand the Ru-catalyzed reactions of the Taxol precursors, we performed calculations (semiempirical, DFT single point energy based on semiempirical geometry, and different DFT methods, also including solvation by toluene) on the diene and dienyne cyclisation reactions of cyclic carbonates **1a** and **1a'**, benzoates **1b** and **1b'**, as well as the experimentally untested acetonides **1c** and **1c'**, catalyzed by the 2nd generation Grubbs catalyst. Previous computational work on Ru-catalyzed ene-ene[7] and ene-yne metathesis reactions[8] had involved a variety of DFT methods, including B3LYP, BP86 and M06 as well as M06L. We chose the latter, which had yielded good results in previous work.[9]

As the complexes involved in the catalytic cycles can assume many different conformations, in each case, Monte-Carlo – type conformational searches were used to identify all possible conformations of the Ru-alkene or Ru-alkyne complexes **2a**-**2c, 2a'**-**2c'**, **3a**-**3c**, and **3a'**-**3c'**. The conformers thus obtained were then all fully optimized using the semiempirical PM6 method. Further stationary points in the catalytic cycles were then derived from the starting Ru-alkene and Ru-alkyne complexes by calculating PM6 reaction profiles for ruthena–cyclobutane and –cyclobutene formation, and ring opening. In case of **1a** and **1a'**, which were most thoroughly investigated, further DFT optimizations were performed at both the M06/SDD and M06L/SDD levels of theory.

Results and Discussion

Evaluation of method performance:

The M06/SDD and M06L/SDD methods seem to perform equally well on the systems investigated, and only minor differences were noted. Figure 2 shows a plot of the M06L/SDD energies of all stationary points optimized for systems **a** and **a'** (cyclic carbonates) vs. the corresponding M06/SDD energies. The correlation is excellent (R^2 = 0.976), and the slope (b = 1.016) only very slightly deviates from the ideal value of b = 1.0.

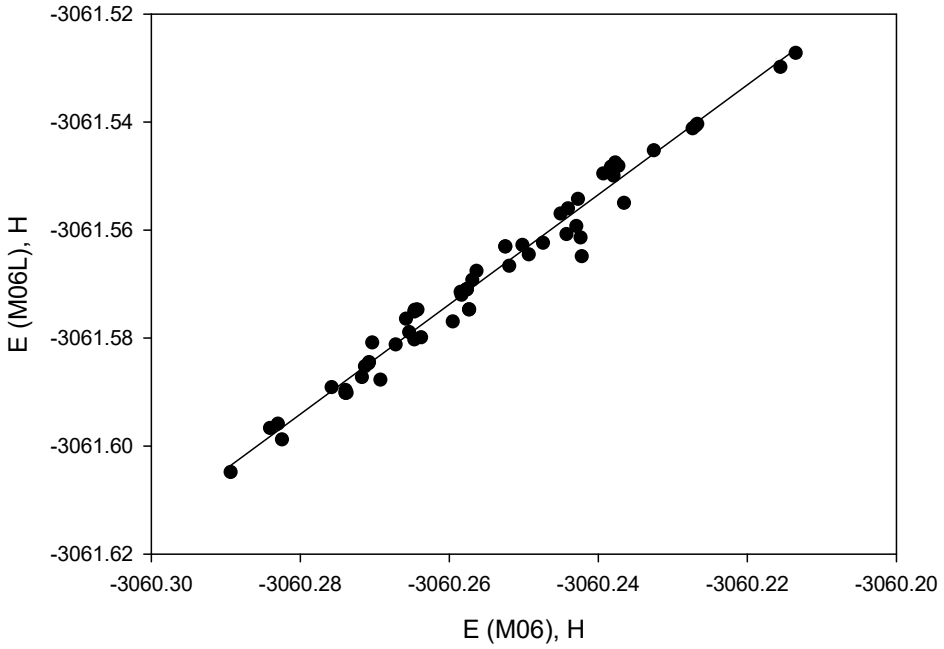

Figure 2: Plot of electronic energies (M06L/SDD) vs. electronic energies (M06/SDD) for a series of conformers of stationary points optimized.

If the PM6 energies are plotted against the M06 energies, the overall correlation is poorer, with a significant deviation from b = 1.0 (R^2 = 0.74, b = 1.161) (Figure 3):

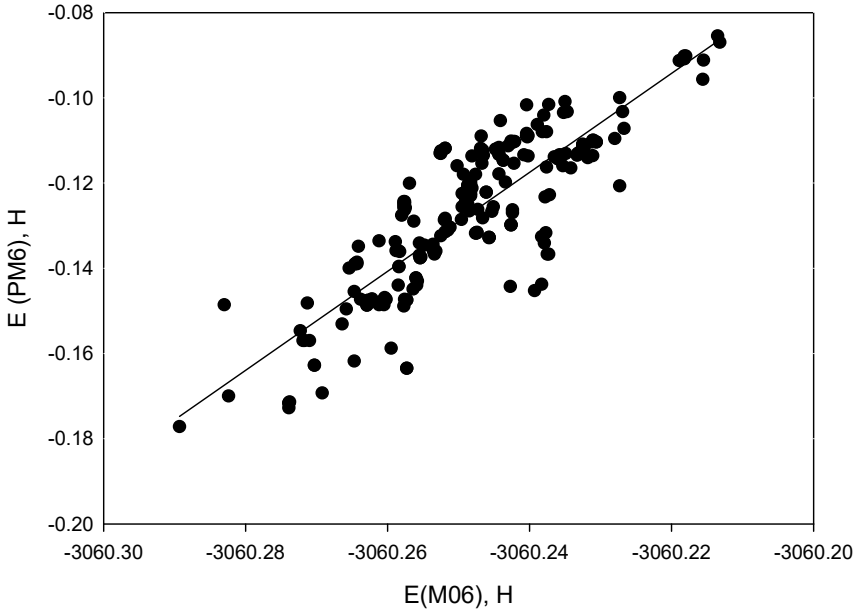

Figure 3: Plot of electronic energies (PM6) vs. electronic energies (M06/SDD) for a series of conformers of stationary points optimized.

The conclusion from this evaluation is that, while M06/SDD and M06L/SDD give comparable results, the much more economical semiempirical PM6 method also tends to qualitatively reproduce the trends. The following discussion will thus be based on the PM6 as well as M06L energies.

Finally, a plot of the M06/SDD(toluene) vs. the M06/SDD energies shows excellent linearity and a slope of unity (R^2 = 0.996, b = 1.002) (Figure 4):

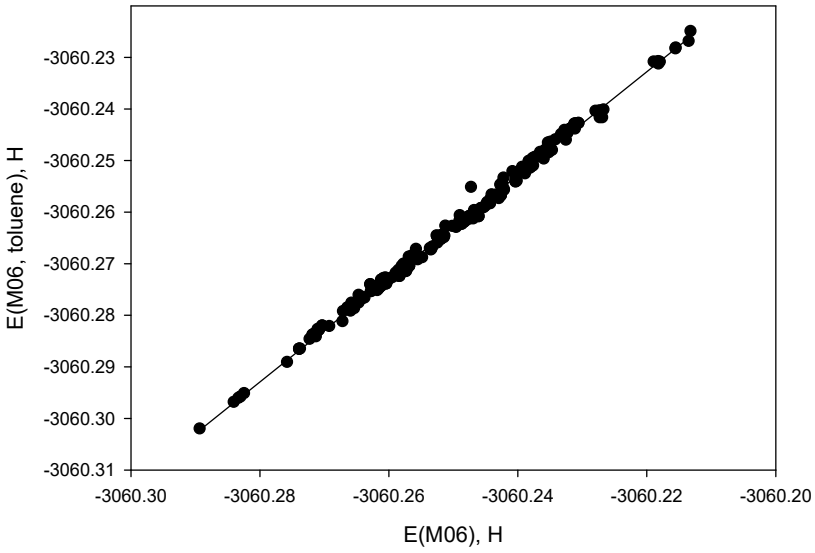

Figure 4: Plot of electronic energies (M06/SDD(scrf,toluene)) vs. electronic energies (M06/SDD) for a series of conformers of stationary points optimized.

This indicates that solvation by toluene stabilizes transition states and minima to a similar degree, and that polar effects very likely do not play an important role.

Calculations on the uncomplexed precursor and product molecules

Initially, calculations were performed on uncomplexed precursors and products to investigate conformational preferences and thermodynamic stabilities. Using Monte-Carlo – type conformational searches at the MMFF force-field level of theory, we generated 100 conformers for each of the two diastereomers **1a** and **1a'**, and all conformers for products *cis*-**2a**, *cis*-**2a'**, *trans*-**2a**, *trans*-**2a'**, **3a**, and **3a'**. The geometries thus obtained were then all further optimized at the M06/6-31G(d) level of theory. From the energetically most favorable conformers of precursor **1a**, exergonic reactions are predicted for formation of Taxol-derivative **3a** (ΔG = -12.3 kcal mol^{-1}) and the lowest energy conformer of cyclooctene *cis*-**2a**, whereas the lowest-energy conformer of *trans*-cyclooctene *trans*-**2a** is predicted to be formed in an endergonic reaction (ΔG = 13.6 kcal mol^{-1}) (Scheme 2). Similarly, starting from diastereomer **1a'**, Taxol-derivative **3a'** (ΔG = -25.3 kcal mol^{-1}) and *cis*-cyclooctene *cis*-**2a'** (ΔG = -3.6 kcal mol^{-1}) are formed in exergonic reactions, whereas *trans*-cyclooctene *trans*-**2a'** (ΔG = 11.4 kcal mol^{-1}) (Scheme 3) is again formed endergonically. As side product, isobutene is formed in all reactions. Hence, the calculations on the uncomplexed precursor and product molecules alone are consistent with the experimental observations, as the thermodynamic preference for Taxol formation in fact is predicted to be significantly higher in system **1a'**. However, as the experimental observations clearly indicate that the catalytic cycle is not under thermodynamic control, calculations were also performed on the intermediates and transition states involved in the catalytic cycles.

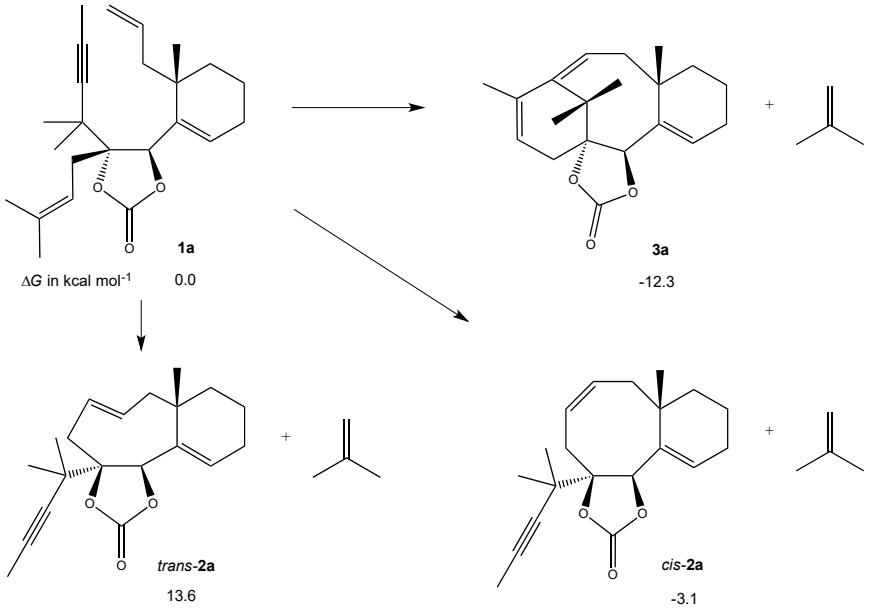

Scheme 2: Free enthalpies of reaction for the formation of products from precursor **1a** (M06/6-31G(d), relative to **1a** = 0.0 kcal mol^{-1}).

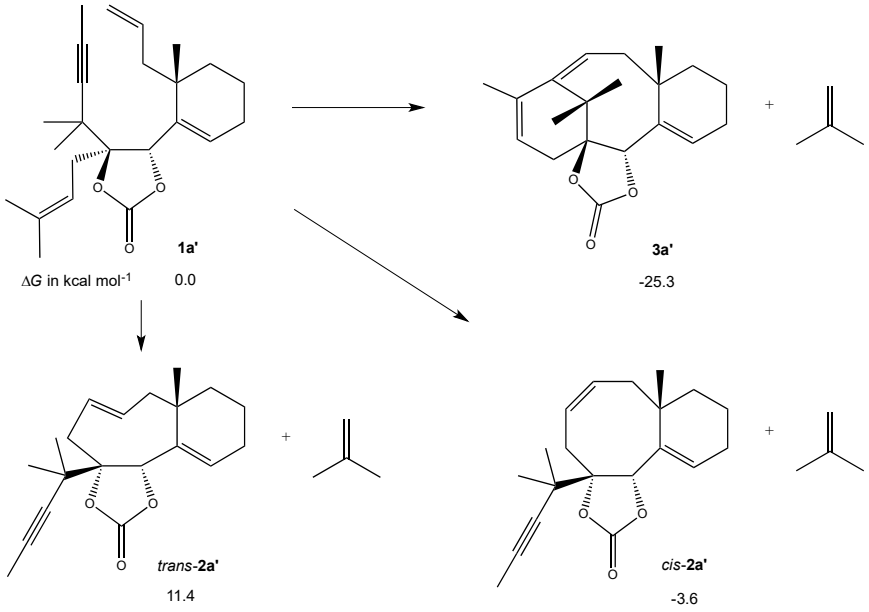

Scheme 3: Free enthalpies of reaction for the formation of products from precursor **1a'** (M06/6-31G(d), relative to **1a'** = 0.0 kcal mol^{-1}).

Calculations on the ruthenium-catalyzed reactions of cyclic carbonates (systems a and a')

The following schemes 4-7 show the stationary points and transition structures investigated.

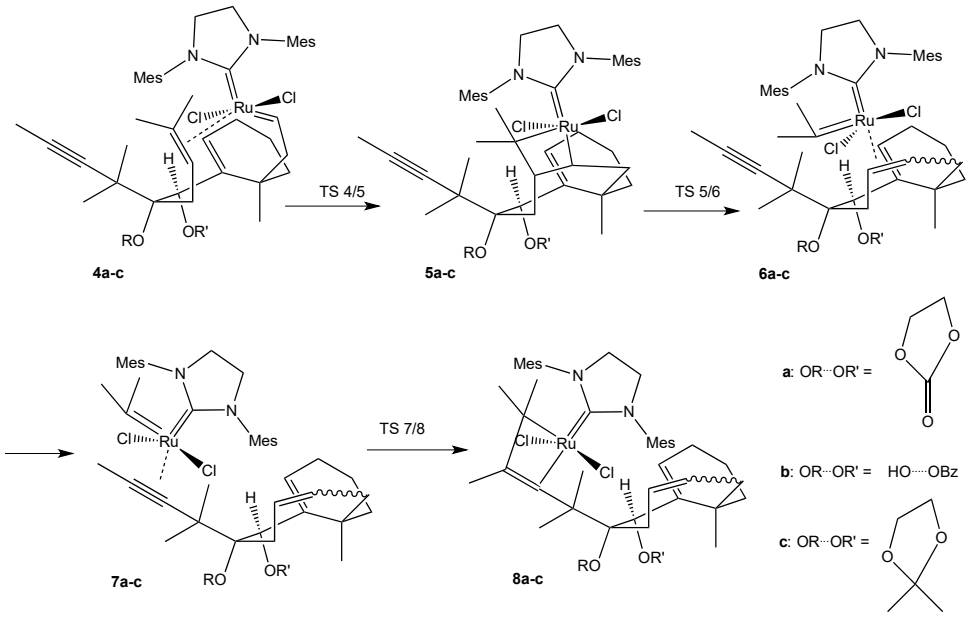

Scheme 4: Structures of stationary points in diene metathesis reaction calculated for systems **a** (cyclic carbonate), **b** (mono-benzoate), and **c** (acetonide)

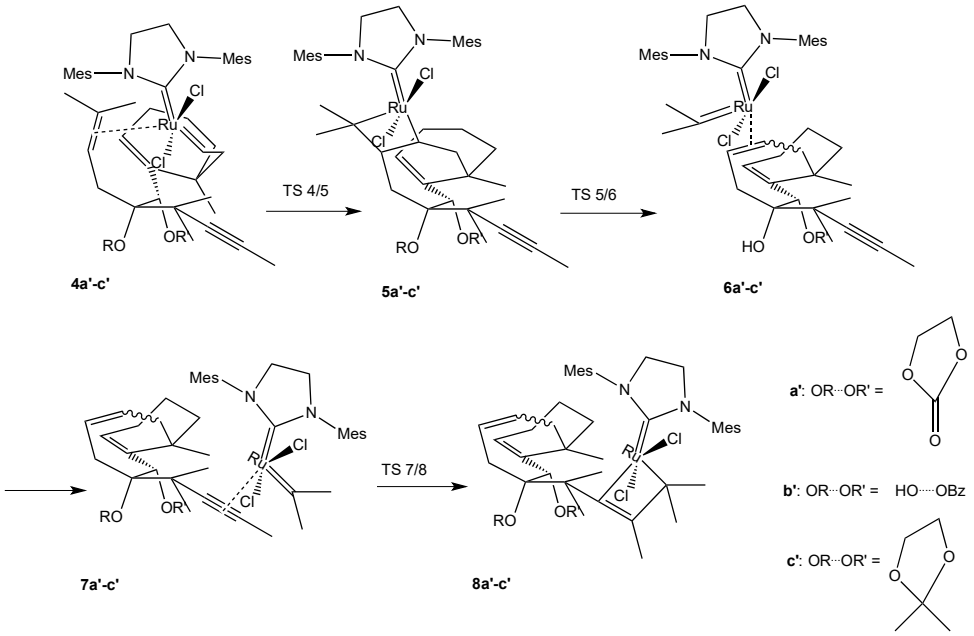

Scheme 5: Structures of stationary points calculated for diene metathesis reaction for systems **a'** (cyclic carbonate, other diastereomer), **b'** (mono-benzoate, other diastereomer), and **c'** (acetonide, other diastereomer)

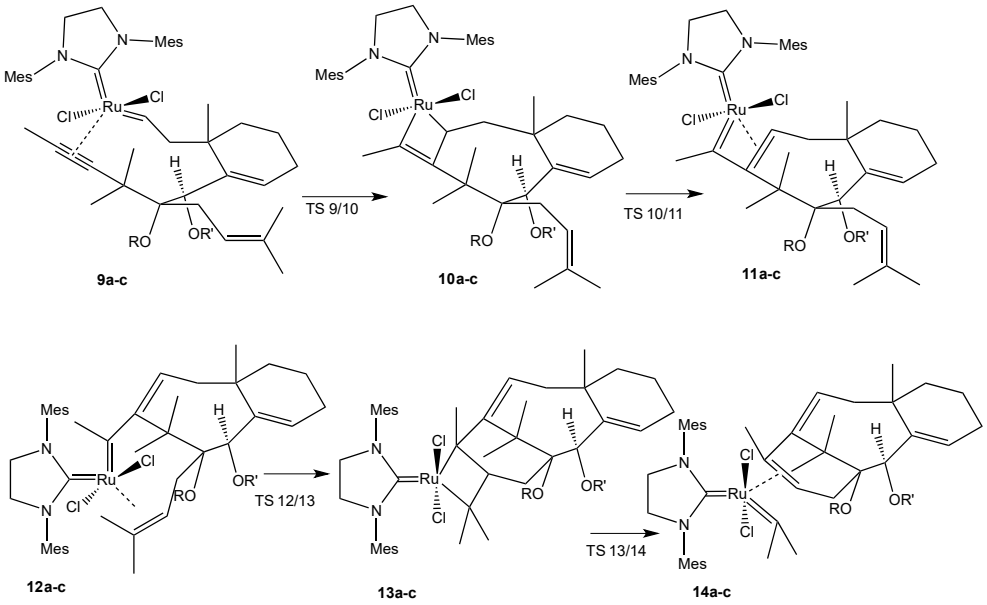

Scheme 6: Structures of stationary points in dienyne metathesis reaction calculated for systems **a** (cyclic carbonate), **b** (mono-benzoate), and **c** (acetonide). For the definition of OR and OR', see Schemes 4, 5 or 7.

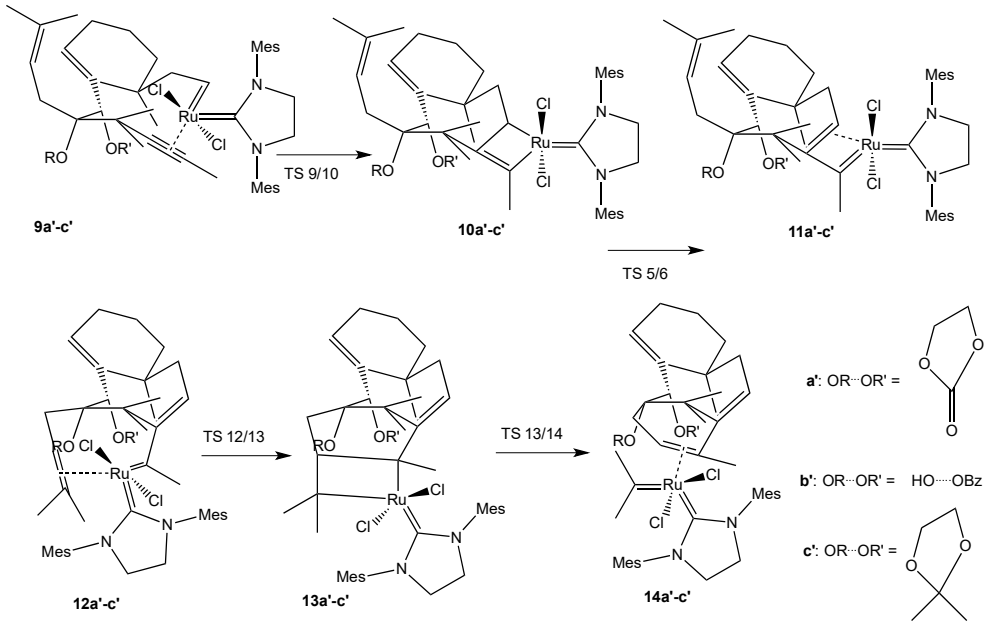

Scheme 7: Structures of stationary points in dienyne metathesis reaction calculated for systems **a'** (cyclic carbonate, other diastereomer), **b'** (mono-benzoate, other diastereomer), and **c'** (acetonide, other diastereomer).

In all calculations, the tricyclohexylphosphine ligand present in the original 2nd generation Grubbs catalyst was omitted, as it is not involved in stabilisation of any active species. For both systems **a** and **a'**, we calculated the Ru-catalyzed diene ring-closing metathesis (RCM) reactions (Schemes 4 and 5) and the dienyne cascade reactions resulting in formation of Taxol derivatives (Schemes 6 and 7). In case of the diene RCM, the cyclooctene products **6a** and **6a'** can be formed as *cis*- or *trans*-isomers. In order to check for the stabilisation of the *cis*- or *trans*-cyclooctenes by coordination to ruthenium, we additionally calculated the alkyne complexes **7a**/**a'** and the isomeric ruthenacyclobutenes **8a**/**a'**. No attempt was made at localizing any stationary points connecting **6a/a'** with **7a/a'**, as the conformational change would have involved too many degrees of freedom. For the same reason no attempts were made to computationally describe the conformational rearrangement linking the Ru-dienylidene **11a/a'** and the Ru-alkene complex **12a/a'** in case of the dienyne RCM cascade reaction (Schemes 6 and 7). When using PM6 theory, Ru-dienylidenes **11a/a'** could not be localised as minimum structures, attempts at optimization resulted in the ruthenacyclobutenes instead. Also, the transition states linking **10a/a'** and **11a/a'** could not be localised with any method.

The results of the calculations are summarized in Figures 5 – 7. It is noted that only some of the reactive species, namely the ruthenium-alkene and ruthenium-alkyne complexes **6**, **7**, and **14**, can serve as exit points from the catalytic cycle, whereas loss of the ruthenium-containing fragment is not possible for any other reactive species calculated. To read Figures 5 -7, please start from the middle. The starting points are structures **4** and **9**. To the right, the reaction coordinate for ene-ene metathesis is found, to the left, the reaction coordinate for ene-yne-ene metathesis.

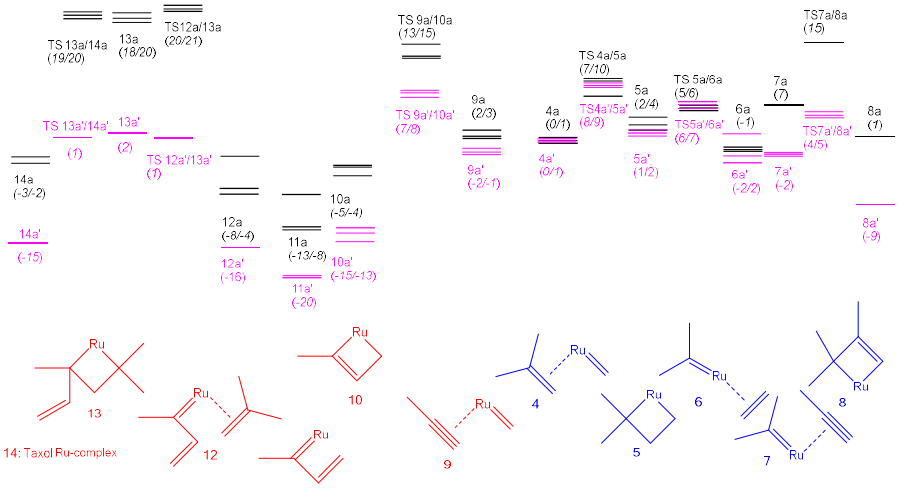

Figure 5: Calculated reaction coordinates for formation of **6a**/**8a** and Taxol derivative **14a** (black) as well as **6a'**/**8a'** and Taxol derivative **14a'** (magenta) (M06L/SDD). The structures shown represent the reactive core only, for full structures see Schemes 4 and 6. Structures shown in blue belong to the reaction coordinate for ene-ene metathesis (cyclooctene formation), structures shown in red belong to the

reaction coordinate for ene-yne-ene metathesis (formation of Taxol derivatives**)**. The horizontal lines indicate the relative Gibbs free energies (*T* = 298 K) of the three lowest-energy conformers.[10] The numbers shown give the range of energies in kcal mol^{-1}, relative to the lowest-energy conformer of **4a**/**4a'**. Ruthenacyclobutane **13a'** is calculated to be higher in free energy than either TS **12a'**/**13a'** or TS **13a'**/**14a'**. This is due to entropic contributions. In terms of enthalpy alone, the ruthenacyclobutane **13a'** is a shallow minimum.

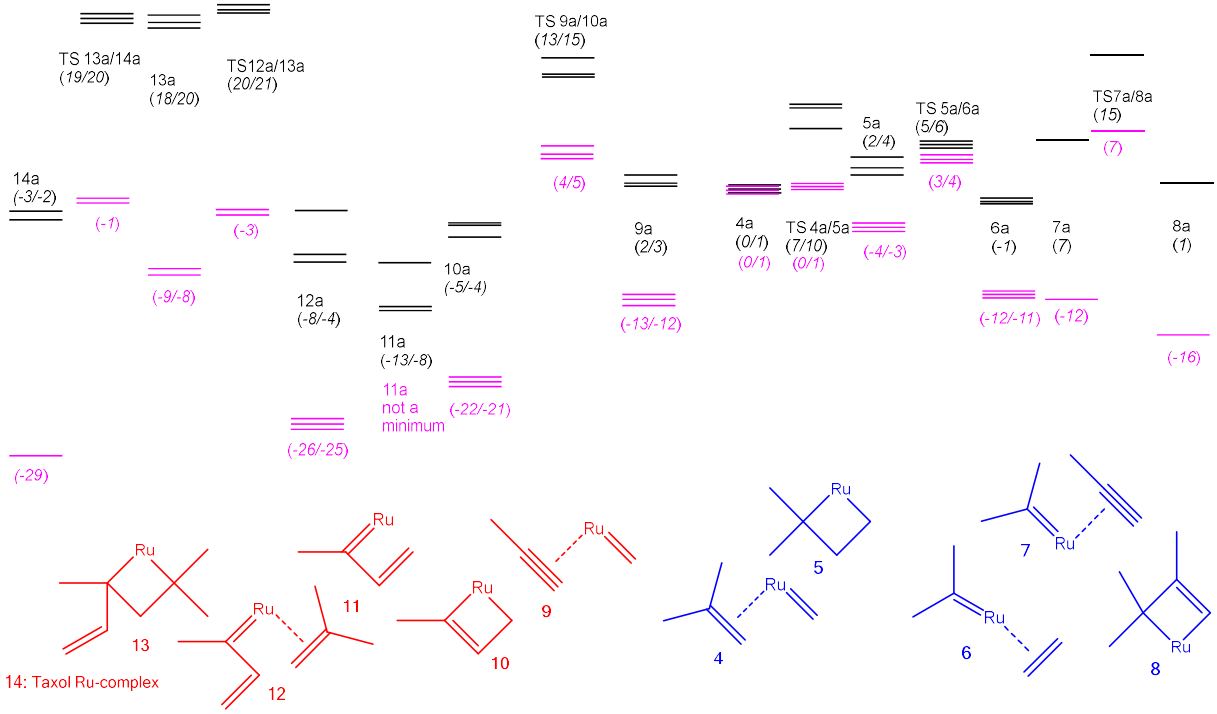

Figure 6: Calculated reaction coordinates for formation of **6a**/**8a** and Taxol derivative **14a**. Data shown in black: M06L/SDD. Data shown in magenta: PM6. The structures shown represent the reactive core only, for full structures see Schemes 4 and 6. Structures shown in blue belong to the reaction coordinate leading to formation of **6a**/**7a**, structures shown in red lead to Taxol derivative **14a**. The horizontal lines indicate the relative Gibbs free energies (*T* = 298 K) of the three lowest-energy conformers.[10] The numbers shown give the range of energies in kcal mol^{-1}, relative to the lowest-energy conformer of **4a**.

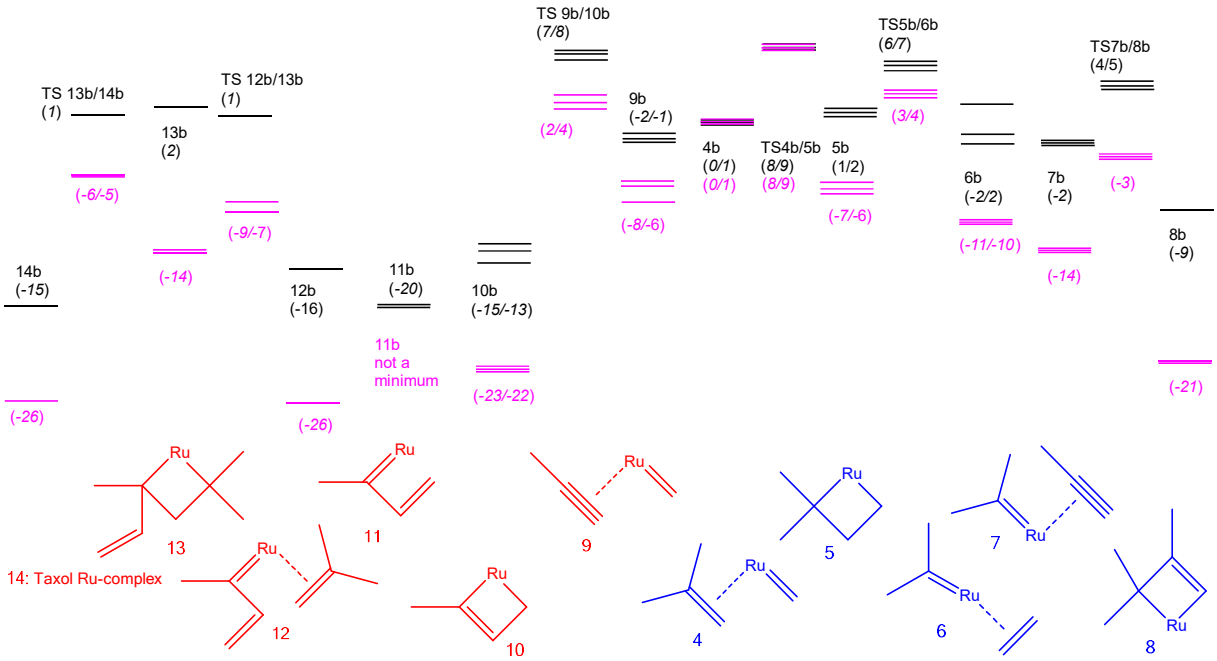

Figure 7: Calculated reaction coordinates for formation of **6a'**/**8a'** and Taxol derivative **14a'**. Data shown in black: M06L/SDD. Data shown in magenta: PM6. The structures shown represent the reactive core only, for full structures see Schemes 4 and 6. Structures shown in blue belong to the reaction coordinate leading to formation of **6a'**/**7a'**, structures shown in red lead to Taxol derivative **14a'**. The horizontal lines indicate the relative Gibbs free energies (T = 298 K) of the three lowest-energy conformers.[10] The numbers shown give the range of energies in kcal mol^{-1}, relative to the lowest-energy conformer of **4a'**.

A comparison of Figures 5-7 reveals that in each case, formation of the Taxol derivative **14** would be the outcome of a reaction under thermodynamic reaction control. The reaction product predicted to be formed under kinetic reaction control, however, differs between isomers **a** and **a'**. Using both the PM6 and the M06L level of theory, isomer **a** is calculated to preferentially result in formation of the undesired product **6a**/**7a**, whereas formation of Taxol derivative **14a'** is both thermodynamically and kinetically favorable for isomer **a'** – in full agreement with the experimental findings, which also conclude that the reaction must occur under kinetic reaction control.[6a] The results obtained by DFT and PM6 differ in that PM6 appears to significantly underestimate the barriers involved in the diene metathesis reaction, and it overestimates the stability of the ruthenium-alkyne complexes, if the DFT calculations are taken as benchmark. Nevertheless, it is encouraging that the experimental findings are qualitatively reproduced even using the inexpensive PM6 method.

Using equation (1), we can estimate rate constants for some of the reactions involved in the catalytic cycles.

$$k = (\mathrm{k}T / \mathrm{h}) \times \exp(\Delta S^{\ddagger} / \mathrm{R}) \times \exp(-\Delta H^{\ddagger} / \mathrm{R}T) \quad \textit{(eq. 1)}$$

At the reaction temperature used in the experimental work (refluxing toluene, T = 384 K), the activation enthalpy (M06L: $\Delta H^{\ddagger}$ = 24.8 kcal mol^{-1}) and activation entropy (M06L: $\Delta S^{\ddagger}$ = -12.3 cal mol^{-1} K^{-1}) for the rate-determining step in the formation of **14a** (**12a** → **13a**), in combination with the unfavorable equilibrium constant (K_{12a} = 0.001) in the equilibrium **12 a** / **11a** translate into a rate constant k = 1.8 × 10^{-7} s^{-1}, corresponding to a lifetime τ ~ 1600 h for the reaction **11a** → **12a** → **13a**. This analysis rationalises the failure in experimentally converting the unwanted isomer **2a** into **3a**, using the 2nd generation Grubbs catalyst under prolonged heating or use of higher temperatures.[6a] In case of the formation of **6a**, the same analysis needs to be applied to the reaction **4a** → **5a**, which is the rate determining step along this reaction coordinate. Alkene complex **4a**, however, is in a very unfavorable equilibrium with the global minimum Ru-dienylidene **11a** (K_{4a} = 4 × 10^{-8}). The calculated activation parameters (M06L: $\Delta H^{\ddagger}$ = 5.3 kcal mol^{-1}, $\Delta S^{\ddagger}$ = -7.2 cal mol^{-1} K^{-1}) for this reaction thus translate into a rate constant k = 0.5 s^{-1} at T = 384 K. The short lifetime thus predicted for **4a** in the presence of the active form of the 2nd generation Grubbs catalyst indicates that it is not the metathesis reaction itself that is the actual rate-determining step in the experiment, but rather loss of tricyclohexylphosphine from the catalyst, generating the catalytically active species, or loss of the active ruthenium center from either **6a** or **7a**. This would be in line with previous findings.[11]

In case of isomer **a'**, an analogous analysis allows for an estimation of the rate constants of the rate determining steps. The rate determining step in the reaction coordinate of the formation of ruthenium complex **14a'** is the conversion of **12a'** into **13a'**, which is preceded by an equilibrium **11a'**/**12a'**, again favouring the dienylidene **11a'**. The calculated activation parameters (M06L: $\Delta H^{\ddagger}$ = 16.4 kcal mol^{-1}, $\Delta S^{\ddagger}$ = -5.3 cal mol^{-1} K^{-1}) in combination with the equilibrium constant (K_{12b} = 0.005) yield a rate constant k = 1.3 s^{-1} at T = 384 K, which might indicate that it is again another process such as regeneration of active catalyst that is the actual rate determining step here. The same also applies in all likelihood to the formation of **6a'**/**7a'**, for which the rate determining step in the calculated reaction coordinate is **4a'** → **5a'.** As **4a'** again is in an unfavorable equilibrium with the global minimum **11a'**, the very low equilibrium concentration of **4a'** ($K_{4a'}$ = 4 × 10^{-12}) needs to be taken into account, turning the formation of **6a'**/**7a'** into a relatively slow process (k = 3.0 × 10^{-4} s^{-1} at T = 384 K corresponding to τ = 54 min), in spite of a small activation enthalpy and only moderately negative activation entropy for this step in the diene metathesis reaction (M06L: $\Delta H^{\ddagger}$ = 4.3 kcal mol^{-1}, $\Delta S^{\ddagger}$ = -11.8 cal mol^{-1} K^{-1}).

In order to elucidate the reasons for the predicted selectivities, we need to investigate structural aspects of the species present in the active cycles. Figure 8 shows optimized structures (M06L/SDD) of stationary points (lowest energy conformers of minima and transition structures) in the formation of **6a**.

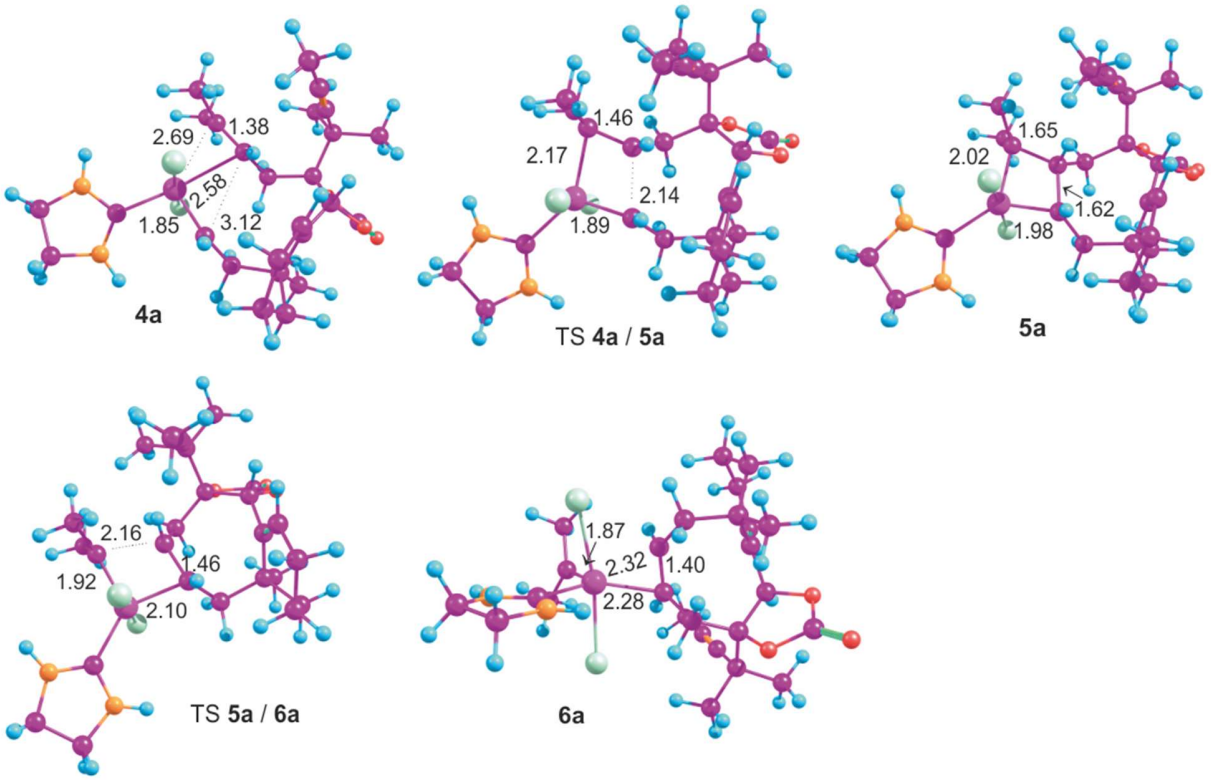

Figure 8: Optimized structures (M06L/SDD) of stationary points in the formation of **6a**. Top left: **4a**. Top middle: TS **4a**/**5a**. Top right: **5a**. Bottom left: TS **5a**/**6a**. Bottom right: **6a**. Bond lengths given are in Å. For the sake of clarity, the mesityl groups in the NHC ligand (although part of the geometry optimization) have been replaced by hydrogen atoms in this Figure. For the coordinates of the full structures, see the Supporting Information.

As seen in Figure 8, the C=C bond of the alkene moiety bound to the Ru centre initially is oriented perpendicular to the Cl-Ru-Cl axis. After the ruthenacyclobutane is cleaved again, the C=C bond of the *cis*-cyclooctene **6a** formed rotates to be parallel to the Cl-Ru-Cl axis, with significantly shorter bonds between the Ru and the carbon atoms of the C=C bond serving as ligand. Attaining this orientation, which has also been found to be favorable in previous computational work on Ru-catalysed alkene metathesis reactions,[9a] might serve to provide driving force for the reaction. The C-C distances in the transition structures are typical for Ru-catalyzed diene ring closing metathesis reactions, e.g., TS **4a**/**5a**, the newly forming Ru-C bond is calculated as r_{Ru-C} = 2.14 Å, where previous work on the TS of the Hoveyda-Grubbs catalyst with 1-hexene gave r_{Ru-C} = 2.15 Å.[9a]

The stationary points localized along the reaction coordinate leading to **6a'**/**7a'** are similar to the stationary point shown in Figs. 8/8S, with one important difference: in this system, the lowest-energy conformer of the initial Ru-alkene complex **4a'** is predicted to preferentially show an orientation that leads to formation of a Ru-cyclooctene complex **6a'** exhibiting a *trans* double bond in the eight-membered ring. Likewise, the lowest-energy conformers of the initial transition state TS **4a'**/**5a'**, the ruthenacyclobutane **5a'** and the second transition state TS **5a'**/**6a'** would all lead to a *trans*-cyclooctene.

Only at the stage of the final alkene complex **6a'**, the lowest energy isomer is a *cis*-cyclooctene. Hence, the diene metathesis reaction in system **a'** is not only disfavored because it is outcompeted by a facile dienyne metathesis sequence, it also, under full kinetic control, would yield an unfavourable strained *trans*-cyclooctene as product. Relatively low-lying conformers leading to a *cis*-cycloctene complex do exist, but are higher in energy than the most favorable conformers resulting in a *trans*-cyclooctene by ca. 1.5 kcal mol^{-1} (M06L/SDD), for **4a'**, TS **4a'/5a'**, **5a'**, and TS **5a'/6a'**. At the stage of the final Ru-cyclooctene complex **6a'**, the most stable conformer of the Ru-*cis*-cyclooctene complex *cis*-**6a'** is calculated (M06L/SDD) to be more stable than the lowest-energy conformer of *trans*-**6a'** by 10.1 kcal mol^{-1}. As the energy difference (M06/6-31G(d): 11.4 kcal mol^{-1}) calculated for the uncomplexed products is similar, this indicates that complexation to the ruthenium center does not stabilise the more reactive *trans*-cyclooctene over the *cis*-cyclooctene to a large degree. It is also noted that the most stable conformer of optimized *cis*-**6a'** has the alkene moiety coordinated to the ruthenium atom oriented perpendicular to the Cl-Ru-Cl axis. Figure 9 shows relevant stationary points (without mesityl groups for clarity).

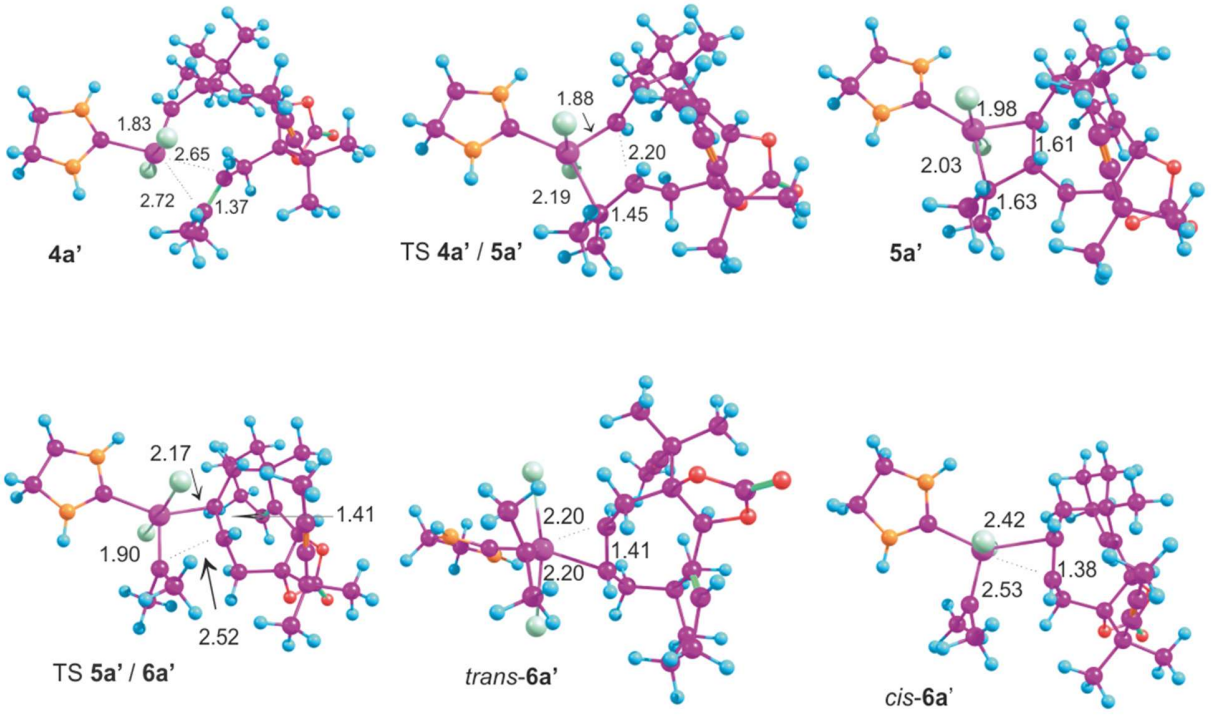

Figure 9: Optimized structures (M06L/SDD) of stationary points in the formation of **6a'**. Top left: **4a'**. Top middle: TS **4a'/5a'**. Top right: **5a'**. Bottom left: TS **5a'/6a'**. Bottom middle: *trans*-**6a'** (formed kinetically). Bottom right: *cis*-**6a'**. Bond lengths given are in Å. For the sake of clarity, the mesityl groups in the NHC ligand (although part of the geometry optimization) have been replaced by hydrogen atoms in this Figure. Please note the different perspectives used for *trans*-**6a'** and *cis*-**6a'**. For the coordinates of the full structures, see the Supporting Information.

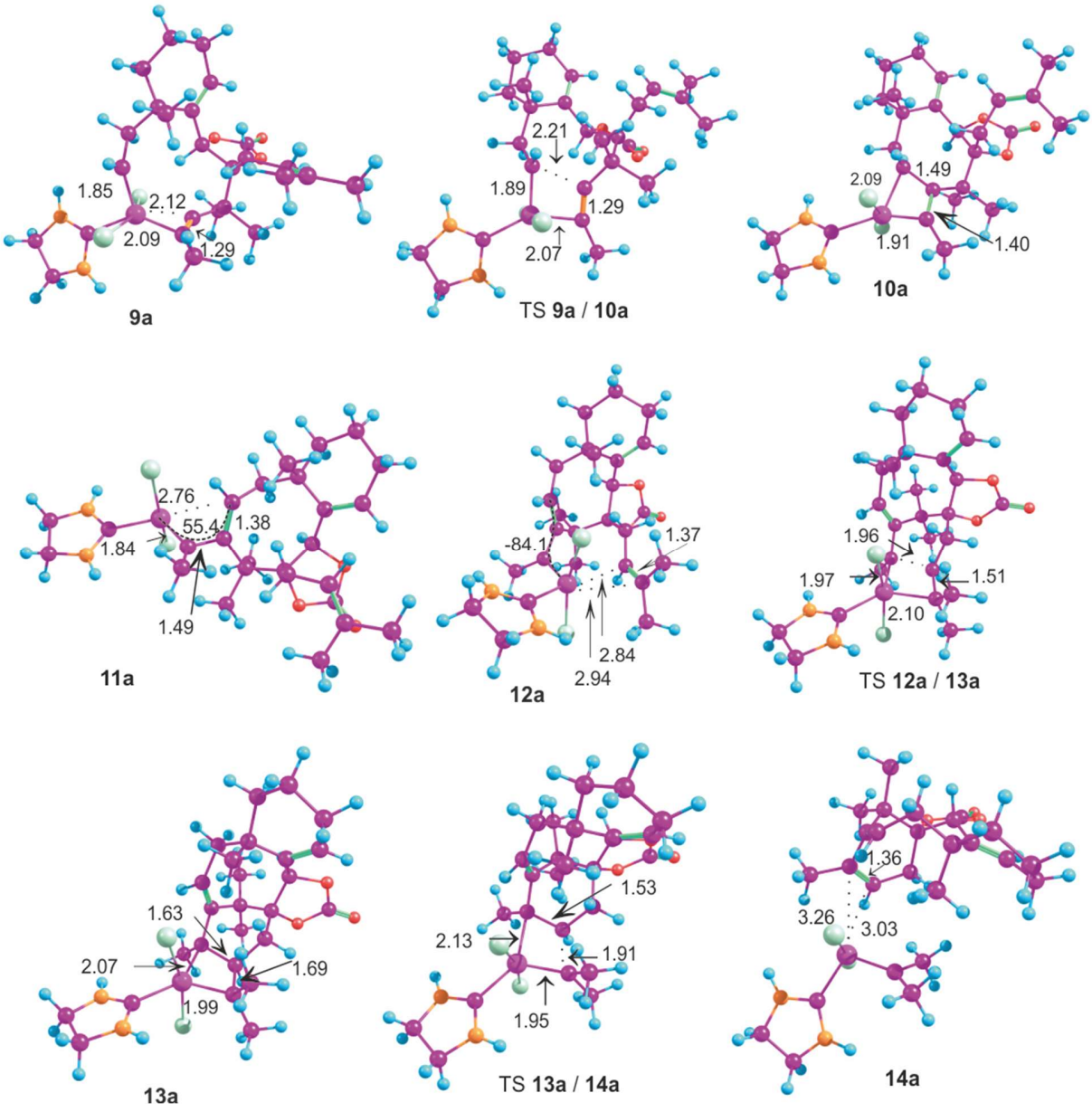

Figure 10: Optimized structures (M06L/SDD) of stationary points in the formation of **14a**. Top left: **9a**. Top middle: TS **9a**/**10a**. Top right: **10a**. Middle left: **11a**. Middle middle: **12a**. Middle right: TS **12a**/**13a**. Bottom left: **13a**. Bottom middle: TS **13a**/**14a**. Bottom right: **14a**. Bond lengths given are in Å, dihedral angles in °. For the sake of clarity, the mesityl groups in the NHC ligand (although part of the geometry optimization) have been replaced by hydrogen atoms in this Figure. For the coordinates of the full structures, see the Supporting Information.

In case of the dienyne metathesis reaction of system **a** (Figure 10), the C≡C bond in the initial Ru-alkyne complex **9a** is preferentially oriented parallel to the Cl-Ru-Cl axis. Hence, for formation of ruthenacyclobutene **10a**, the C≡C ligand needs to rotate by 90°. Given the rigidity of the molecule, this likely is associated with significant energetic cost, and therefore it offers an explanation for the relatively

high barrier predicted for this reaction step. The lowest-energy species along the reaction coordinate is ruthena-dienylidene complex **11a**, in which the C=C bond is rotated out of the Ru=C-C plane by 55.4°. No transition state could be localised for interconversion of **10a** and **11a**. Relaxed surface scans resulted in dependencies of energy vs. reaction coordinate that behaved in a non-continuous fashion, even if broken-symmetry wavefunctions were employed, and did not allow us to localise a well-defined maximum-energy geometry that could have been taken as starting guess for a transition state optimization. While this might be taken as evidence for a surface-crossing mechanism, we note that both **10a** and **11a** proved to be well-behaved closed-shell singlet states without triplet instability. In terms of Woodward-Hoffmann terminology, the reaction **10a** $\rightarrow$ **11a** corresponds to a 4-electron electrocyclic ring opening reaction, which in a concerted mechanism would have to proceed in conrotational fashion. As the presence of the chloride ligands makes this concerted reaction pathway impossible (the $RuCl_2$ moiety would have to rotate as a whole, which could not work for steric reasons), a biradical intermediate, possibly on the triplet surface, may therefore be involved. No attempts were made to explore high-spin potential energy surfaces in this system.

For a continuation of the reaction along the reaction coordinate to **14a**, the low-energy dienylidene complex **11a** needs to convert endothermically into the Ru-alkene complex **12a**, in which the Ru=C and C=C bonds of the ruthenadiene unit are decoupled, as evidenced by a Ru=C-C=C dihedral of -84.1°. Formation of the ruthenacyclobutane **13a** is an unfavourable process. Apart from the large barrier calculated for this process, a clear indicator for this is the extraordinarily long C-C$(CH_3)_2$ bond found here. A calculated value of $r_{C\text{-}C}$ = 1.69 Å is outwith the normal range of C-C bond lengths,[12] and it is indicative of the significant amount of strain that needs to be built up in the formation of this four-membered ring. The final Ru-alkene complex **14a** shows very long Ru-C bonds, indicating that the Taxol derivative formed will only be loosely bound to the Ru atom, providing a good exit point for the sequence. Figure 10 shows relevant optimized geometries.

The reaction coordinate yielding **14a'** shows stationary points similar to those predicted for system **a**. Again, the initial Ru-alkyne complex **9a'** preferentially has the C≡C bond of the alkyne ligand oriented parallel to the Cl-Ru-Cl axis, and again, the alkyne ligand therefore has to rotate by 90° for the metathesis reaction to occur. The Ru-dienylidene complex **11a'** by far is the lowest energy species along the reaction coordinate, and again, no transition structure could be located connecting ruthenacyclobutane **10a'** and ruthenadienylidene **11a'**. In system **a'**, the ruthenacyclobutane **13a'** is only a minimum structure, if entropic contributions (at T = 384K) are ignored. Figure 11 shows the simplified optimized geometries.

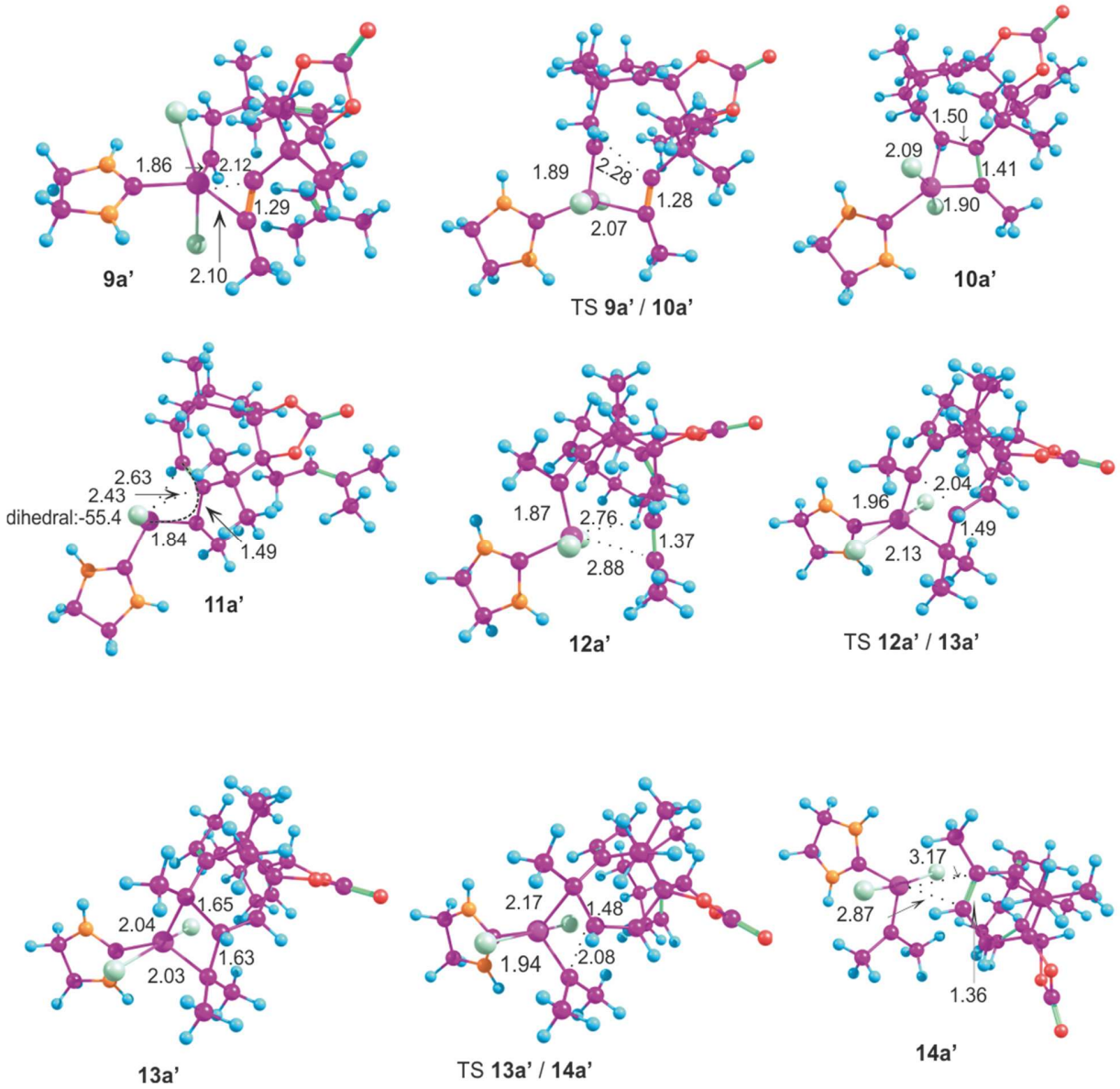

Figure 11: Optimized structures (M06L/SDD) of stationary points in the formation of **14a'**. Top left: **9a'**. Top middle: TS **9a'/10a'**. Top right: **10a'**. Middle left: **11a'**. Middle middle: **12a'**. Middle right: TS **12a'/13a'**. Bottom left: **13a'**. Bottom middle: TS **13a'/14a'**. Bottom right: **14a'**. Bond lengths given are in Å, dihedral angles in °. For the sake of clarity, the mesityl groups in the NHC ligand (although part of the geometry optimization) have been replaced by hydrogen atoms in this Figure. For the coordinates of the full structures, see the Supporting Information.

The reason for the dienyne cascade reaction being favored for precursor **1a'**, while **1a** yields the undesired product of diene metathesis, likely rests in the varying degrees of stability of the final ruthenacyclobutane intermediates **13a** and **13a'**. The reactive center is sterically overloaded in both systems. The decisive structural difference between **13a** and **13a'** probably lies in the orientation of the pseudoaxial methyl substituent present in the cyclohexene ring, which in **13a'** points away from the

reactive center, but in **13a** points toward it, thus further constraining the space available. In order to test this hypothesis, we optimized (M06L/SDD) structures **11d**, **11d'**, **13d**, and **13d'**, corresponding to the lowest-energy conformers of **11a**, **11a'**, **13a**, and **13a'**, but with the pseudoaxial cyclohexene methyl group replaced by a hydrogen atom. The results show that for both systems **d** (ΔG = 9 kcal mol^{-1}) and **d'** (ΔG = 19 kcal mol^{-1}), the energy difference favoring the ruthenadienylidene **11** over the ruthenacyclobutane **13** should be smaller than for **a** (ΔG = 31 kcal mol^{-1}) and **a'** (ΔG = 22 kcal mol^{-1}). It does not come as a surprise that the effect of omitting the cyclohexene methyl group should be significantly larger for the system in which this methyl group points to the reactive center, as in **a**, as opposed to the system in which it is a remote methyl group (as in **a'**).

Calculations on the ruthenium-catalyzed reactions of benzoates and acetonides (systems b, b', c, and c')

The ruthenium-catalyzed reactions of benzoate systems **b** and **b'**, which had experimentally been demonstrated to yield the cyclooctene products of a diene metathesis reaction,[6a] and the acetonide systems **c** and **c'** (experimentally untested) were also studied. In order to minimise CPU time requirements, these systems were investigated employing semiempirical PM6 theory, which, when applied to systems **a** and **a'**, had yielded results in qualitative agreement with the results of more demanding DFT calculations. In case of the systems **b** and **b**', a few selected stationary points were further optimized at the M06L/SDD level of theory. For the structures of the minima investigated, see Schemes 4-7. It is noted that a few stationary points could not be optimized at the M06L level of theory. In one case (TS **5b'/6b'**), TS optimizations for several conformers consistently failed because of C-Me rotations in the mesityl groups showing imaginary frequencies of a similar magnitude to the reaction coordinate desired. Even using extremely fine integration grids, this obstacle could not be overcome. In other cases (**6b'**, **14b'**), the alkene complexes were so sterically overloaded that minima could no longer be optimized.

Figure 12 shows the results (M06L/SDD) obtained for the benzoate systems **b** and **b'**. Again, this Figure is read from the middle, with **4** and **9** as starting points for ene-ene metathesis (blue core structures) and ene-yne-ene metathesis (red core structures).

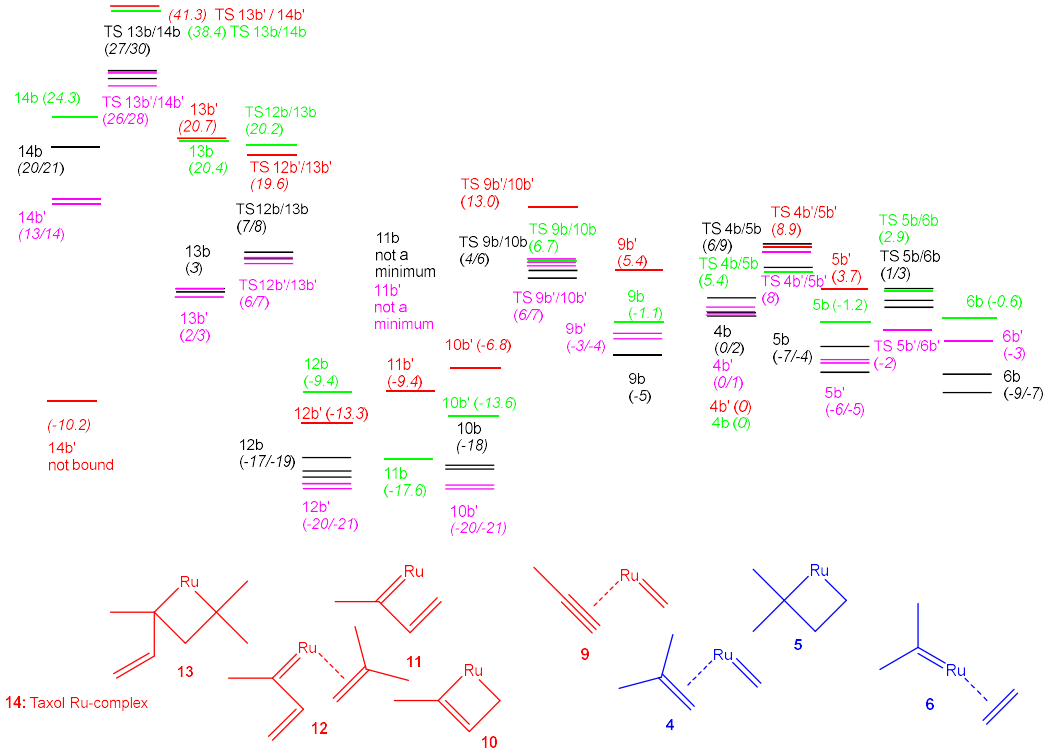

Figure 12: Calculated reaction coordinates for formation of **6b**/**8b** and Taxol derivative **14b** (PM6) (in black); (M06L/SDD) (in green) as well as for formation of **6b'**/**8b'** and Taxol derivative **14b'** (PM6) (in magenta); (M06L/SDD) (in red). The structures shown represent the reactive core only, for full structures see Schemes 4 and 6. Structures shown in blue belong to the reaction coordinate leading to formation of **6b**/**7b** and **6b'**/**7b'**, structures shown in red lead to Taxol derivative **14b**/**14b'**. The horizontal lines indicate the relative Gibbs free energies (T = 298 K) of the lowest three conformers.[10] The numbers shown give the range of energies in kcal mol^{-1}, relative to the lowest-energy conformer of **4b**/**4b'**.

While there are significant differences between the DFT results and the results obtained PM6 theory (e.g., PM6 overestimating the stability of the ruthenacyclopropanes in the taxol forming branch), the methods agree on the essential finding. For both system **b** and **b'**, the preferred reaction route, by a wide margin, is diene metathesis, yielding cyclooctenes **6b** and **6b'**. The alternative dienyne metathesis cascade reaction is predicted to be more favourable in the initial stages of the catalytic cycle, as the ruthenacyclobutenes **10b/b'** and/or the ruthenadienylidenes **11b/b'** are calculated to be the lowest energy species in the entire system. (But again, the ruthenadienylidenes **11b/b'** are not predicted to be minima at the semiempirical level of theory.) However, the follow-up ring-closing reactions to yield Taxol Ru-complexes **14b/b'** are predicted to be thermodynamically very unfavorable, and also to suffer from prohibitively high barriers of in excess of 40 kcal mol^{-1} (PM6; M06L/SDD), from **10b/b'**. We note that for both Ru-cyclooctene complex **6b** and **6b'**, our M06L/SDD optimizations predict preferential *cis*-stereochemistry at the cyclooctene C=C bond being formed, in agreement with experimental findings, whereas semiempirical PM6 theory predicts preferential formation of a *trans*-cyclooctene.

Given the larger size of a benzoate protective group, as opposed to a cyclic carbonate, the very high energy of the ruthenacyclobutane intermediates **13b** and **13b'** crucial for generating **14b** or **14b'** does not come as a surprise. The failure in experimentally converting either diastereomer of **1b** into **14b** thus most likely results from a steric overload of the reactive centre, destabilising **13b** and **13b'** to a degree that **14b** or **14b'** can only be formed by crossing very high energy transition states.

Our results (PM6) for the acetonide systems **c** and **c'** are shown in the Supporting Information. They reveal that the acetonide systems **c** and **c'** should mirror the cyclic carbonates **a** and **a'**, in that the diastereomer **c** is predicted to behave like **a**, with preferential diene ring closing metathesis occurring due to very high barriers in the final steps of the dienyne metathesis route. In case of system **c'**, again the barriers in tricycle formation are smaller, and preferential formation of Taxol derivative complex **14c'** should occur. The cyclooctenes formed in the ene-ene metathesis reactions are predicted to be a *cis*-cyclooctene for system **c**. In case of system **c'**, again a *trans*-cyclooctene is predicted to be formed.

Conclusion

Calculations on the ene-ene and ene-yne-ene ring closing metathesis reactions in Taxol derivatives synthesis, employing both density functional theory (M06L) and a semiempirical method (PM6), yield results in agreement with the results of recent experimental work. As the reactive centres in the catalytic intermediates are sterically highly overloaded, even small differences in the size of peripheral protecting groups (cyclic carbonate vs. benzoate) play a decisive role in determining chemoselectivity. Compact cyclic diol protecting groups like cyclic carbonate or acetonide are predicted to favor the desired ene-yne-ene cascade reaction for one of the precursor diastereomers, whereas the more bulky monobenzoate protecting group is predicted to result in cyclooctene formation (ene-ene RCM) for both diastereomers. PM6 theory, while overestimating some barriers, is found to qualitatively reproduce the results obtained using DFT.

Computational methodology

Employing Spartan software version 14,[13] we initially generated libraries of a maximum of 100 conformers each for **1a**, **1a'**, **2a**, **2a**', **3a**, and **3a**', using a Monte-Carlo – type conformational search routine with the MMFF[14] force field. All conformers of **1a**, **1a'**, **2a**, **2a**', **3a**, and **3a**' were subsequently further optimized at the M06/6-31G(d) level[15,16] of theory. For the stationary points involved in the catalytic cycles, libraries of conformers (up to 100) of **4**(a-c), **4**(a-c)', **9**(a-c), and **9**(a-c)' were similarly generated. In case of systems **a** and **a'**, all conformers were then further optimized, initially at the PM6,[17] then at the M06L/SDD,[18,19] and some also at the M06/SDD level of theory. The influence of solvation by toluene was evaluated for some stationary points by performing single point energy calculations (M06/SDD, polarisable continuum model (Gaussian key word scrf=pcm),[20] based on the M06/SDD gas phase geometries. All geometry optimizations were performed employing the *Gaussian09* suite of programs.[21] In case of systems **b** and **b'**, optimization of all conformers was first conducted at the PM6 level of theory, followed by optimization of the lowest energy conformers using M06L/SDD. For **c**, and **c'**, optimization was limited to PM6 theory. Further stationary points in the catalytic cycles were then obtained starting from all conformers of **4** or **9**, by performing relaxed surface scans (PM6) along

the reaction coordinates desired, using the maximum energy geometries obtained in the relaxed surface scans to fully optimize (first PM6, then DFT (systems a and a')) the transition structures required for all conformers. As the reaction coordinates could be clearly discerned from the imaginary frequency vibrational mode obtained, in all cases, no IRC calculations were performed. Similarly, starting geometries for optimization of subsequent minima (e.g, **5** or **10**) were also obtained from the relaxed surface scans. Free energies given refer to a temperature of *T* = 298 K. In case of systems **b** and **b'**, the lowest energy conformers as obtained by PM6 theory were also further optimized at the M06L/SDD level of theory.

Acknowledgements

Financial support for this work was provided by the University of Glasgow. We thank Dr. Brian Millward, Honorary Research Fellow, for a generous donation. GB, SB, and GC thank the EPSRC UK National Service for Computational Chemistry Software (NSCCS) for a CPU time grant.

Keywords: density functional calculations • Taxol • ring-closing metathesis • ruthenium • semiempirical calculations

Supporting information for this article is given free of charge via: xxxxx

Electronic energies of all stationary points optimized, results for system **c**/**c'**.

Cartesian coordinates are available via the document Coord.xyz, which can be viewed using chemical visualization software.

References

[1] https://news.bms.com/news/details/2021/Bristol-Myers-Squibb-Reports-Fourth-Quarter-and-Full-Year-Financial-Results-for-2020/default.aspx (accessed 23 June 2021).
[2] Yared, J. A.; Tkaczuk, K. H. R. Update on taxane development: new analogs and new formulations. *Drug Design, Development and Therapy* **2012**, 371-384.
[3] a) Holton, R. A.; Somoza, C.; Kim, H. B.; Liang, F; Biediger, R. J.; Boatman, P. D.; Shindo, M; Smith, C. C.; Kim, S. First total synthesis of taxol. 1. Functionalization of the B ring. *J. Am. Chem. Soc.* **1994**, *116*, 1597-1598; b) Holton, R. A.; Kim, H. B.; Somoza, C.; Liang, F.; Biediger, R. J.; Boatman, P. D.; Shindo, M.; Smith, C. C.; Kim, S. First total synthesis of taxol. 2. Completion of the C and D rings. *J. Am. Chem. Soc.* **1994**, *116*, 1599-1600; c) Nicolaou, K. C.; Yang, Z.; Liu, J. J.; Ueno, H.; Nantermet, P. G.; Guy, R. K.; Claiborne, C. F.; Renaud, J.; Couladouros, E. A.; Paulvannan, K.; Sorensen, E. J. Total synthesis of taxol. *Nature* **1994**, *367*, 630-634; d) Masters, J. J.; Link, J.T.; Snyder, L. B.; Young, W. B.; Danishefsky, S. J. A Total Synthesis of Taxol. *Angew. Chem. Int. Ed.* **1995**, 34, 1723-1726; e) Wender, P. A.; Badham, N. F.; Conway, S. P.; Floreancig, P. E.; Glass, T. E.; Gränicher, C.; Houze, J. B.; Jänichen, J.; Lee, D.; Marquess, D. G.; McGrane, P.L.; Meng, W.; Mucciaro, T. P.; Mühlebach, M.; Natchus, M. G.; Paulsen, H.; Rawlins, D. B.; Satkofsky, J.; Shuker, A.J.; Sutton, J. C.; Taylor, R. E.; Tomooka, K. The Pinene Path to Taxanes. 5. Sterocontrolled Synthesis of a Versatile Taxane Precursor. *J. Am. Chem. Soc.* **1997**, *119*, 2755-

2756; f) Wender, P. A.; Badham, N. F.; Conway, S. P.; Floreancig, P. E.; Glass, T. E.; Houze, J.B.; Krauss, N. E.; Lee, D.; Marquess, D. G.; McGrane, P.L.; Meng, W.; Natchus, M. G.; Shuker, A. J.; Sutton, J. C.; Taylor, R. E. The Pinene Path to Taxanes. 6. A Concise Sterecontrolled Synthesis of Taxol. *J. Am. Chem. Soc.* **1997**, *119*, 2757-2758; g) Mukaiyama, T.; Shiina, I.; Iwadare, H.; Sakoh, H.; Tani, Y.; Hasegawa, M.; Saitoh, K. Asymmetric Total Synthesis of Taxol®. *Proc. Jpn. Acad.* **1997***, 73B*, 95-100; h) Morihara, K.; Hara, R.; Kawahara, S.; Nishimori, T.; Nakamura, N.; Kusama, H.; Kuwajima, I. Total Synthesis of Taxol. *J. Am. Chem. Soc.* **1998**, *120*, 12980-12981; i) Kanda, Y.; Nakamura, H.; Umemiya, S.; Puthukanoori, R. K.; Appala, V. R. M.; Gaddamanugu, G. K.; Paraselli, B. R.; Baran, P. S. Two-Phase Synthesis of Taxol. *J. Am. Chem. Soc.*, **2020**, *142*, 10526-10533.

[4] a) Doi, T.; Fuse, S.; Miyamoto, S.; Nakai, K.; Sasuga, D.; Takahashi, T. A Formal Total Synthesis of Taxol Aided by an Automated Synthesizer. *Chem. Asian J.* **2006**, *1*, 370-383; b) Hirai, S.; Utsugi, M.; Iwamoto, M.; Nakada, M. Formal Total Synthesis of (–)-Taxol through Pd-Catalyzed Eight-membered Carbocyclic Ring Formation. *Chem. Eur. J.* **2015**, *21*, 355-359; c) Fukaya, K.; Tanaka, Y.; Sato, A. C.; Kodama, K.; Yamazaki, H.; Ishimoto, T.; Nozaki, Y.; Iwaki, Y. M.; Yuki, Y.; Umei, K.; Sugai, T.; Yamaguchi, Y.; Watanabe, A.; Oishi, T.; Sato, T.; Chida, N. Synthesis of Paclitaxel. 1. Synthesis of the ABC ring of Paclitaxel by SmI_2-Mediated Cyclization. *Org. Lett.* **2015**, *17*, 2570-2573; d) Fukaya, K.; Kodama, K.; Tanaka, Y.; Yamazaki, H.; Sugai, T.; Yamaguchi, Y.; Watanabe, A.; Oishi, T.; Sato, T.; Chida, N. Synthesis of Paclitaxel. 2. Construction of the ABCD Ring and Formal Synthesis. *Org. Lett.* **2015**, *17*, 2574-2577.

[5] a) Muller, B.; Delaloge, F.; den Hartog, M.; Férézou, J.-P.; Pancrazi, A.; Prunet, J.; Lallemand, J.-Y.; Neuman, A.; Prangé, T. Diastereoselective Synthesis of a Taxane Precursor. *Tetrahedron Lett*. **1996**, *37*, 3313-3316; b) Muller, B.; Férézou, J.-P.; Lallemand, J.-Y.; Pancrazi, A.; Prunet, J.; Prangé, T. "Abnormal" Eight-Membered Ring Formation through S_N2' Intramolecular Nozaki/Kishi Reaction in a Synthetic Approach to a Taxane Precursor. *Tetrahedron Lett.* **1998**, *39*, 279-282; c) Bourgeois, D.; Lallemand, J.-Y.; Pancrazi, A.; Prunet, J. Diastereoselective Synthesis of a seco-Taxane. *Synlett* **1999**, 1555-1558; d) Bourgeois, D.; Maiti, G.; Pancrazi, A.; Prunet, J. Diastereoselective Additions of Nucleophiles to Hindered α-Trimethylsilyloxy Aldehydes. *Synlett* **2000**, 323-326; e) Bourgeois, D.; Pancrazi, A.; Ricard, L.; Prunet, J. Synthesis of Highly Functionalized Cyclooctenes by Ring-Closing Metathesis: Unexpected Formation of a trans Isomer. *Angew. Chem.* **2000**, *112*, 741-744; *Angew. Chem. Int. Ed.* **2000**, *39*, 725-728; f) Bourgeois, D.; Mahuteau, J.; Pancrazi, A.; Nolan, S. P.; Prunet, J. Synthesis of BC Ring-Systems of Taxol by Ring-Closing Metathesis. *Synthesis* **2000**, 869-882.

[6] a) Letort, A.; Aouzal, R.; Ma, C.; Long, D.-L.; Prunet, J. Highly Efficient Synthesis of the Tricyclic Core of Taxol by Cascade Metathesis. *Org. Lett*. **2014**, *16*, 3300-3303; b) Ma, C.; Letort, A.; Aouzal, R.; Wilkes, A.; Maiti, G.; Farrugia, L. J.; Ricard, L.; Prunet, J. Cascade Metathesis Reactions for the Synthesis of Taxane and Isotaxane Derivatives. *Chem. Eur. J.* **2016**, *22*, 6891-6898; c) Letort, A.; Long, D.-L.; Prunet, J. Study of Cascade Ring-Closing Metathesis Reactions en Route to an Advanced Intermediate of Taxol. *J. Org. Chem*. **2016**, *81*, 12318-12331.

[7] a) Vyboishchikov, S. F.; Thiel, W. Ring Closing Olefin Metathesis Reactions on Ruthenium Carbene Complexes: Model DFT Study of Stereochemistry. *Chem. Eur. J.* **2005**, *11*, 3921-3935. b) Solans-Monfort, X.; Pleixats, R.; Sodupe, M. DFT Mechanistic Study on Diene Metathesis Catalyzed by Ru-Based Grubbs-Hoveyda-Type Carbenes: The Key Role of π-Electron Delocalization in the Hoveyda Ligand. *Chem. Eur. J.* **2010**, *16*, 7331-7343.

[8] Nuñez-Zarur, F.; Solans-Monfort, X.; Rodríguez-Santiago, L.; Pleixats, R.; Sodupe, M. Mechanistic Insights Into Ring-Closing Enyne Metathesis with the Second Generation Grubbs-Hoveyda Catalyst: A DFT Study. *Chem. Eur. J*. **2011**, *17*, 7506-7520.
[9] a) Ashworth, I. W.; Hillier, I. H.; Nelson, D. J.; Percy, J. M.; Vincent, M. A. Olefin Metathesis by Grubbs-Hoveyda Complexes: Computational and Experimental Studies of the Mechanism and Substrate-Dependent Kinetics. *ACS Catal.* **2013**, *3*, 1929-1939. b) Poater, A.; Pump, E.; Vummaleti, S. V. C.; Cavallo, L. The Right Computational Recipe for Olefin Metathesis with Ru-Based Catalysts: The Whole Mechanism of Ring-Closing Olefin Metathesis. *J. Chem. Theory Comput.* **2014**, *10*, 4442-4448.
[10] A maximum of three conformers is given, which are up to 5 kcal mol^{-1} above the lowest-energy conformer.
[11] a) Benitez, D.; Tkatchouk, E.; Goddard, W. A. Conformational Analysis of Olefin-Carbene Ruthenium Metathesis Catalysts. *Organometallics* **2009**, *28*, 2643-2645; b) Sanford, M. S.; Love, J. A.; Grubbs, R. H. Mechanism and activity of ruthenium olefin metathesis catalysts. *J. Am. Chem. Soc.* **2001**, *123*, 6543-6554; c) Sanford, M. S.; Ulman, M.; Grubbs, R. H. New Insights into the Mechanism of Ruthenium-Catalyzed Olefin Metathesis Reactions. *J. Am. Chem. Soc.* **2001**, *123*, 749-750.
[12] This is similar to the length of the central C-C bond in the sterically highly overloaded hexakis-(3,5-di-*tert*-butylphenyl)ethane, see a) Kahr, B.; van Engen, D.; Mislow, K. Length of the ethane bond in hexaphenylethane and its derivatives. *J. Am. Chem. Soc.* **1986**, *108*, 8305-8307, and b) Grimme, S.; Schreiner, P. R. Steric Crowding Can Stabilize a Labile Molecule: Solving the Hexaphenylethane Riddle. *Angew. Chem. Int. Ed*. **2011**, *50*, 12639-12642.
[13] Spartan 14, Vers. 1.1.8, Wavefunction Inc., Irvine, CA.
[14] Halgren, T. A. Merck molecular force field. I. Basis, form, scope, parametrization, and performance of MMFF94. *J. Comput. Chem.* **1996**, 490-519.
[15] Zhao, Y.; Truhlar, D. G. The M06 suite of density functionals for main group thermochemistry, thermochemical kinetics, noncovalent interactions, excited states, and transition elements: two new functionals and systematic testing of four M06-class functionals and 12 other functionals. *Theor. Chem. Acc.* **2008**, *120*, 215-241.
[16] Ditchfield, R.; Hehre, W. J.; People, J. A. Self-Consistent Molecular-Orbital Methods. IX. An extended Gaussian-Type Basis for Molecular-Orbital Studies of Organic Molecules. *J. Chem. Phys.* **1971**, *54*, 724-728.
[17] Stewart, J. J. P. Optimization of parameters for semiempirical methods V: Modification of NDDO approximations and application to 70 elements. *J. Mol. Model.* **2007**, 1173-1213.
[18] Zhao, Y.; Truhlar, D. G. A new local density functional for main-group thermochemistry, transition metal bonding, thermochemical kinetics, and noncovalent interactions. *J. Chem. Phys.* **2006**, *125*, 194101.
[19] a) Dunning, T.H., Jr.; Hay, P. J. Gaussian Basis Sets for Molecular Calculations in *Modern Theoretical Chemistry*, Ed. H. F. Schaefer III, Vol. 3 (Plenum, New York, 1977) 1-27. b) Andrae, D.; Häussermann, U. Energy-adjusted *ab initio* pseudoinitials for the second and third row transition elements. *Theor. Chem. Acc.* **1990**, *77*, 123-141.
[20] Tomasi, J. ; Mennucci, B. ; Cammi, R. Quantum Mechanical Continuum Solvation Models. *Chem. Rev.* **2005**, 105, 2999-3093.

[21] Gaussian 16, Revision B.01, Frisch, M. J.; Trucks, G. W.; Schlegel, H. B.; Scuseria, G. E.; Robb, M. A.; Cheeseman, J. R.; Scalmani, G.; Barone, V.; Petersson, G. A.; Nakatsuji, H.; Li, X.; Caricato, M.; Marenich, A. V.; Bloino, J.; Janesko, B. G.; Gomperts, R.; Mennucci, B.; Hratchian, H. P.; Ortiz, J. V.; Izmaylov, A. F.; Sonnenberg, J. L.; Williams-Young, D.; Ding, F.; Lipparini, F.; Egidi, F.; Goings, J.; Peng, B.; Petrone, A.; Henderson, T.; Ranasinghe, D.; Zakrzewski, V. G.; Gao, J.; Rega, N.; Zheng, G.; Liang, W.; Hada, M.; Ehara, M.; Toyota, K.; Fukuda, R.; Hasegawa, J.; Ishida, M.; Nakajima, T.; Honda, Y.; Kitao, O.; Nakai, H.; Vreven, T.; Throssell, K.; Montgomery, J. A., Jr.; Peralta, J. E.; Ogliaro, F.; Bearpark, M. J.; Heyd, J. J.; Brothers, E. N.; Kudin, K. N.; Staroverov, V. N.; Keith, T. A.; Kobayashi, R.; Normand, J.; Raghavachari, K.; Rendell, A. P.; Burant, J. C.; Iyengar, S. S.; Tomasi, J.; Cossi, M.; Millam, J. M.; Klene, M.; Adamo, C.; Cammi, R.; Ochterski, J. W.; Martin, R. L.; Morokuma, K.; Farkas, O.; Foresman, J. B.; Fox, D. J. Gaussian, Inc., Wallingford CT, 2016.